The Journal of Infectious Diseases

MAJOR ARTICLE

Inferring Diagnostic Serial Intervals to Understand COVID-19 Transmission Dynamics in Hong Kong and Mainland China

M. Pear Hossain,[1,2] Dongxuan Chen,[1,2] Amy Yeung,[1,2] Dillon C. Adam,[1,2] Wey Wen Lim,[1,2] Yiu Chung Lau,[1,2] Eric H. Y. Lau,[1,2] Jessica Y. Wong,[1] Faith Ho,[1] Huizhi Gao,[1] Lin Wang,[3] Zhanwei Du,[1,2] Peng Wu,[1,2] Benjamin J. Cowling,[1,2] and Sheikh Taslim Ali[1,2]

[1]WHO Collaborating Centre for Infectious Disease Epidemiology and Control, School of Public Health, Li Ka Shing Faculty of Medicine, The University of Hong Kong, Hong Kong Special Administrative Region, China; [2]Laboratory of Data Discovery for Health Limited, Hong Kong Science Park, New Territories, Hong Kong; and [3]Department of Genetics, University of Cambridge, Cambridge, United Kingdom

Background. Estimating the instantaneous reproduction numbers (R_t) requires inferring generation time (*GT*, the interval between successive infections in the transmission chain), often approximated by the serial interval (*SI*, the interval between successive onsets in the transmission chain). The serial interval based on clinical outcomes is subject to recall biases, and such clinical information is not always available. As a comparable metric, we defined the diagnostic serial interval (SI_d, the time between diagnostic reporting of case pairs in a transmission chain) and compared it with the traditional *SI*.

Methods. We analyzed confirmed coronavirus disease 2019 (COVID-19) cases from 3 ancestral waves in Hong Kong and the first wave in mainland China. Using Bayesian methods, we inferred the distributions of effective *SI* and SI_d, along with onset-to-reporting delays, and compared the resulting R_t estimates.

Results. The distributions of *SI* and SI_d were comparable across waves, with shorter means observed in SI_d. Reporting delays for infectors were longer than those for infectees, which was identified as a key factor influencing the temporal variation in *SI* and SI_d. Additionally, factors such as public health and social measures, case profile, and demographics were found to significantly impact the estimates. Time-varying estimates of the reproduction number derived from both *SI* and SI_d were highly consistent, with median absolute differences ranging from 0.12 to 0.19.

Conclusions. The diagnostic serial interval shows potentials as a comparable metric to the traditional serial interval for estimating transmissibility in assessing COVID-19 transmission dynamics, and this approach could be extended for other respiratory viruses.

Keywords. diagnostic serial interval; clinical serial interval; transmissibility; COVID-19; infectious disease.

Along with other key epidemiological parameters, estimating the distributions of the generation time (*GT*, the interval between successive infections in a transmission chain) and the clinical serial interval (*SI*, the interval between successive symptom onsets) is crucial for understanding the transmission dynamics of directly transmitted infectious diseases, including coronavirus disease 2019 (COVID-19) [1–6]. The *GT* distribution is particularly essential for inferring the effective or instantaneous reproduction number (R_t, the average number of secondary cases produced by a primary case at time *t*), which informs real-time public health decision making [7–11]. In practice, because exact infection times are rarely observed, inferring the *GT* is challenging. Consequently, clinical metrics such as the *SI* [12–14] are often used as a proxy for the *GT* distribution. These proxies are subsequently used to estimate the basic (R_0) and time-varying (R_t) reproduction numbers [10, 11, 15, 16], and other transmissibility measures, such as the secondary attack rate, force of infection, and doubling time, etc. [17–20].

However, routinely ascertaining symptom onset dates for cases is not always feasible, and these data are often subject to recall bias, especially during periods of high community transmission [21]. In contrast, case reporting times are frequently recorded with greater precision and are available for a larger proportion of cases. Furthermore, presymptomatic transmission can result in negative *SI* estimates, which are biologically implausible for approximating the *GT* (a strictly positive measure) [14]. Therefore, estimating transmission dynamics based on diagnostic information rather than clinical outcomes may help circumvent these limitations. This provides

Received 28 April 2026; accepted 21 August 2026; published online 26 August 2026

Correspondence: Benjamin J. Cowling, PhD, School of Public Health, LKS Faculty of Medicine, The University of Hong Kong, Patrick Manson Building, 7 Sassoon Road, Pokfulam, Hong Kong SAR-999077, China (bcowling@hku.hk); Sheikh Taslim Ali, PhD, School of Public Health, LKS Faculty of Medicine, The University of Hong Kong, Patrick Manson Building, 7 Sassoon Road, Pokfulam, Hong Kong SAR-999077, China (alist15@hku.hk).

The Journal of Infectious Diseases®

© The Author(s) 2026. Published by Oxford University Press on behalf of Infectious Diseases Society of America.

This is an Open Access article distributed under the terms of the Creative Commons Attribution License (https://creativecommons.org/licenses/by/4.0/), which permits unrestricted reuse, distribution, and reproduction in any medium, provided the original work is properly cited.

https://doi.org/10.1093/infdis/jiag443

Downloaded from academic.oup.com/jid/advance-article/doi/10.1093/infdis/jiag443/8770953 by guest on 06 November 2026

an opportunity to use diagnostic serial interval (SI_d, the time between diagnostic reporting of cases in transmission chain) as a comparable measure to the *SI* and, consequently, as a proxy for the *GT* under a stable surveillance system. Although negative SI_d values are theoretically possible, SI_d relies solely on objective reporting times, which overcomes many limitations of the *SI*, including recall bias [22] (as tests are performed and reported by trained professionals). Additionally, SI_d can be estimated even for asymptomatic infections, which have been reported in varying proportions, ranging from 1% to over 50% for COVID-19 [23]. To our knowledge, the only COVID-19 study to evaluate SI_d was conducted in South Korea, where it was retrospectively estimated using data from early 2020 as an indicator of contact tracing effectiveness [24]. No further studies have explicitly explored temporal characteristics of SI_d and associated factors to illustrate the comparative utility of *SI* and SI_d for estimating R_t. This study aimed to assess the similarity between SI_d and *SI*, using line-list data from ancestral COVID-19 waves in Hong Kong and mainland China during 2020–2021.

METHODS

Data Source and Defining Onsets of the COVID-19 Waves

We obtained line-list data for all laboratory-confirmed COVID-19 cases from the Hong Kong Department of Health including demographics, symptom onset, reporting, isolation or hospital admission dates, infection source, severity, and testing setting. We analyzed the second through fourth waves (up to 23 March 2021), excluding the predominantly imported first wave and the fifth wave, which exceeded contact tracing capacity [25]. For mainland China, we utilized publicly available line-list data for cases reported outside Hubei Province from 1 January to 29 February 2020, sourced from municipal health commissions, as described previously [12, 16, 26, 27]. Detailed wave period definitions and peak timings are provided in the Supplementary Material Section 1 [16, 28]. Statistical analyses were conducted using R version 4.0.5 (R Foundation for Statistical Computing, Vienna, Austria).

Reconstruction of Transmission Pairs and Factor-Based Stratifications

Using line-list and contact tracing information for confirmed COVID-19 cases, we reconstructed transmission pairs following previously reported methods (Supplementary Material Section 2) [12, 27, 28]. To account for factors reported to influence *SI* variation [16, 28–30], we stratified the transmission pair data by temporal and nontemporal characteristics. Temporal stratifications included interwave periods, intrawave periods (prepeak, peak, and postpeak), and transmission generation status (primary, secondary, and tertiary, etc.). Nontemporal factors included case demographics (age [< 65 and ≥ 65 years] and sex), case severity (severe and nonsevere) [31], infection setting (household vs nonhousehold), infection source (local vs imported), and detection setting (private, public, or contract tracing). Additionally, we stratified the data based on infector-specific delays, specifically the isolation delay (defined as the time from symptom onset to isolation) and the reporting delay (defined as the time from symptom onset to case reporting). For both metrics, delays shorter than the respective median were classified as "short," whereas those exceeding the median were designated as "long." For mainland China, stratifications were limited to age, sex, and infection setting (household vs nonhousehold) due to data availability.

Estimation of SI_d, $SI_,$, and Onset-to-Reporting Interval Distributions and Their Temporal Variations

We estimated means, standard deviations, and 95% credible intervals (CrIs) for *SI*, SI_d, and onset-to-reporting delays using Bayesian inference. Parametric distributions (normal, gamma) were fitted to empirical data, with posterior distributions using Markov chain Monte Carlo methods in *rstan* (Supplementary Figure 1 and Supplementary Material Section 3).

We evaluated estimates within stratified subgroups, comparing mean *SI* and SI_d using paired *t* tests, and examining covariates associations using linear regression (Supplementary Material Section 4). Temporal variations were evaluated across epidemic waves and prepeak, peak, and postpeak periods. Time-varying distributions were estimated using a 10-day sliding windows, with 7-day and 14-day in sensitivity analyses (Supplementary Figures 11 and 12). The effective *SI* (forward *SI*) was referenced to the infector's symptom onset [12, 28, 30]. To evaluate reporting delays effects on SI_d, we examined $\Delta = d_1 - d_2$, where d_1 and d_2 are onset-to-reporting delays for infectors and infectees, respectively (Supplementary Material Section 5).

Estimation of R_t Using SI and SI_d

We estimated the effective reproduction number using the *EpiEstim* R package [10, 32], calculating daily incidence (I_t) weighted by infectiousness approximated by time-varying *SI* or SI_d distributions (Supplementary Material Section 6). Because the true infection epidemic curve (epicurve) and *GI* distribution are often unobserved, R_t is typically estimated using reported case counts (reported epicurve) and *SI* distribution. However, *SI* distributions rely on symptom onset, whereas reported epicurves use reporting dates. To assess the impact of these data sources, we compared R_t estimates under 3 combinations: reported epicurve with *SI*, onset epicurve with *SI*, and reported epicurve with SI_d. We additionally estimated R_t using constant retrospective *SI* and SI_d distributions (Supplementary Figure 4). Finally, we conducted a counterfactual analysis simulating 1–4 day earlier or later reporting for

Downloaded from academic.oup.com/jid/advance-article/doi/10.1093/infdis/jiag443/8770953 by guest on 06 November 2026

infectors and infectees to evaluate the impact of reporting delays on SI_d and R_t (Supplementary Figure 5).

Individual-Based Simulation to Assess the Bias in R_t Estimation

To assess bias in R_t estimates using different epidemic curves and interval distributions, we conducted an individual-based simulation based on a Susceptible–Infectious–Recovered (SIR) framework. The model generated infection, symptom onset, and reporting times under prespecified *GT*, incubation period, and reporting delay distributions, allowing reconstruction of infection-, onset-, and report-based epicurves and infector-infectee pairs. From these, we estimated time-varying *GT*, *SI*, and SI_d distributions and corresponding R_t estimates. We also simulated public health and social measures (PHSMs) by reducing onset-to-reporting delays and compared R_t estimates against the reference (infection-based curves with intrinsic *GT*). Bias was quantified using mean squared differences, and sensitivity analyses addressed temporal lag and epidemic-phase thresholds (Supplementary Material Section 7).

RESULTS

During the first 4 waves of COVID-19 in Hong Kong, we could reconstruct 2433 transmission pairs. Of these, 823 were confirmed (including 47, 357, and 355 in the second, third, and fourth waves, respectively, and 64 identified during interwave periods), and the remainder were classified as probable or likely pairs. In mainland China, we reconstructed a total of 629 confirmed pairs during the first wave. Onset-based and reported epicurves showed similar overall trends, although the observed peak timings were delayed by approximately 5–10 days in the reported epicurves across waves (Figure 1*A*–*D*).

The distributions of *SI* and SI_d were comparable across epidemic waves, with shorter means for SI_d than for *SI* (Supplementary Table 1). Similar to the mean *SI*, mean SI_d was significantly shorter across prepeak, peak, and postpeak periods, with shorter means during postpeak periods for each wave except the second wave in Hong Kong. Stratified analyses showed that mean SI_d was significantly shorter than mean *SI* across most factors and subgroups for each wave in Hong Kong. Regression analyses indicated that reporting delay, older age ($\geq$ 65 years), disease severity, and isolation delays significantly influenced *SI* and SI_d (Supplementary Figure 2). Notably, longer isolation and reporting delays tended to lengthen *SI* but shorten SI_d, whereas local transmission and severe disease were associated with longer intervals.

Comparison of Time Varying *SI* and SI_d Estimates

Time-varying *SI* and SI_d distributions were largely comparable in mean estimates and their patterns across waves in Hong Kong and mainland China (Figure 2). In Hong Kong, the mean estimates of effective *SI* and SI_d were found to vary in the same direction during most of the second wave and during some phases of the third and fourth waves, but changed in opposite directions during other phases of the third and fourth waves. The mean daily absolute difference between *SI* and SI_d was 0.40 days (interquartile range [IQR], 0.21–1.03), 1.66 days (IQR, 0.99–2.31), and 1.42 days (IQR, 0.84–1.95) in the second, third, and fourth waves in Hong Kong, respectively, and 0.63 days (IQR, 0.29–1.46) in the first wave in mainland China (Figure 2*A*–*D*).

To evaluate the effect of reporting delays on SI_d, we examined the difference in onset-to-reporting delays between infectors and infectees (Δ) (Supplementary Figure 3). The distributions of Δ were comparable across waves and locations, with mean differences of 0.52 days (IQR, 0.32–0.76), 0.40 days (IQR, 0.16–0.59), and 0.51 days (IQR, 0.19–0.85) for the second, third, and fourth waves in Hong Kong, respectively, and 0.46 days (IQR, 0.30–0.92) for the first wave in mainland China. Overall, temporal estimates of reporting delays showed that infectors generally had longer mean reporting delays than infectees across the waves in Hong Kong, whereas the opposite pattern was observed during the postpeak period of the first wave in mainland China.

Linear regression analyses showed that differences in SI_d were partly explained by reporting delays (d_1 and d_2) (Supplementary Section 5). In models including only d_1 and d_2, these variables explained up to 40% of the variation in SI_d in the second wave, and 21% and 23% in the third and fourth waves, respectively (Supplementary Tables 2–4). After adjustments for additional covariates, the proportion of explained variance increased to 92%, 69%, and 75%, respectively. However, in the combined Hong Kong dataset, the fully adjusted model explained only 53% of the variance in SI_d (Supplementary Table 5).

Impact of *SI* and SI_d on Inferring Time-Varying Transmissibility

Mean estimates of R_t, derived from effective *SI* and SI_d distributions and their respective epicurves (reported and onset-based), showed similar overall temporal patterns with some variation during the early and late phases of epidemic waves (Figure 3). In particular, the estimates of R_t based on SI_d distributions and reported epicurves agreed closely with those based on *SI* and onset epicurves, with median absolute differences (MAD) ranging from 0.12 (IQR, 0.08–0.15) to 0.19 (IQR, 0.10–0.28) across locations and waves (Supplementary Table 6). Similarly, R_t estimates based on *SI* and reported epicurves were comparable to those based on SI_d, with MAD ranging from 0.08 (IQR, 0.04–0.16) to 0.16 (IQR, 0.12–0.18). These findings were consistent when evaluated using dynamic time warping and Euclidean distance and were similar under traditional constant retrospective *SI* and SI_d distributions (Supplementary Figure 4). Sensitivity analyses assuming reporting 1–4 days earlier/later showed that the time-varying

Downloaded from academic.oup.com/jid/advance-article/doi/10.1093/infdis/jiag443/8770953 by guest on 06 November 2026

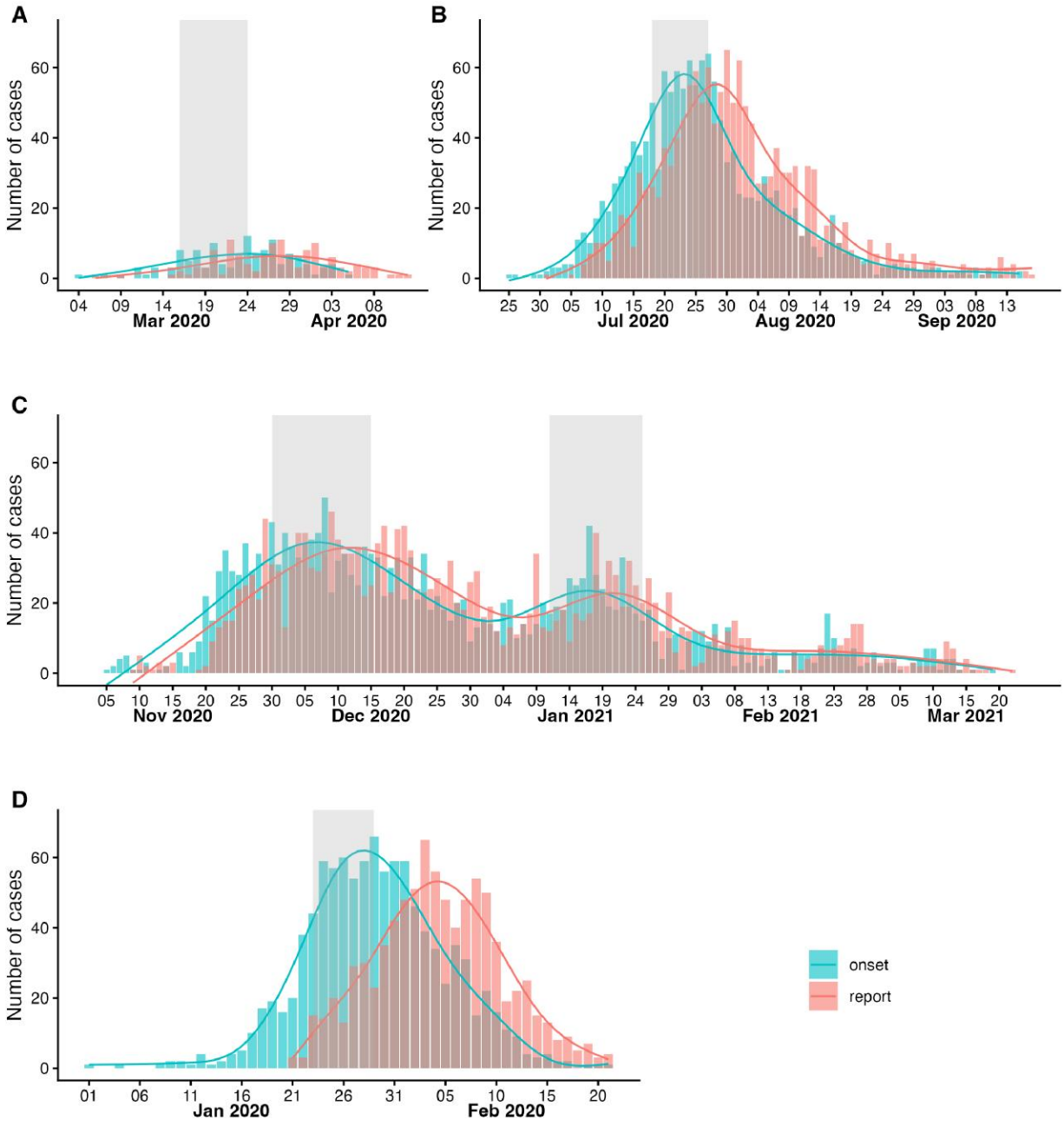


Figure 1. Major epidemic waves in Hong Kong between 1 March 2020 and 23 March 2021 and in mainland China between 1 January and 29 February 2020: (*A*) second wave, (*B*) third wave, and (*C*) fourth wave in Hong Kong, and (*D*) the first wave in mainland China. The epidemic curves were constructed based on the date of symptom onset (blue solid bars) and the date of the reporting confirmed by reverse transcription polymerase chain reaction (RT-PCR) test (red solid bars). The respective solid lines represent smoothed trends fitted with a generalized additive model. The shaded rectangles show the epidemic peak periods for the respective waves.

SI_d estimates were robust, with only minor variation in the mean SI_d, the corresponding 95% CrIs, and daily R_t estimates (Supplementary Figure 5). Absolute changes in SI_d estimates ranged from 0% to 19%, indicating limited sensitivity to reporting-time perturbation.

In simulation analyses, R_t estimates derived from reported epicurves with effective SI_d were comparable to those obtained using the traditional approach under intervention (contact tracing) scenarios with 60% effectiveness (Figure 4*A*–*C*). Relative to reference estimates based on infection epicurves and *GT*, the shortest time to optimal mean squared differences was 6 days for onset epicurves with *SI*, 7 days for reported epicurves with *SI*, and 13 days for reported epicurves with SI_d (Figure 4*D*). These findings were stable when assessed across 50%–100% of simulated datasets and under additional intervention scenarios with 0%, 30%, and 90% effectiveness (Figures 4*E* and Supplementary Figures 6–8).

Downloaded from academic.oup.com/jid/advance-article/doi/10.1093/infdis/jiag443/8770953 by guest on 06 November 2026

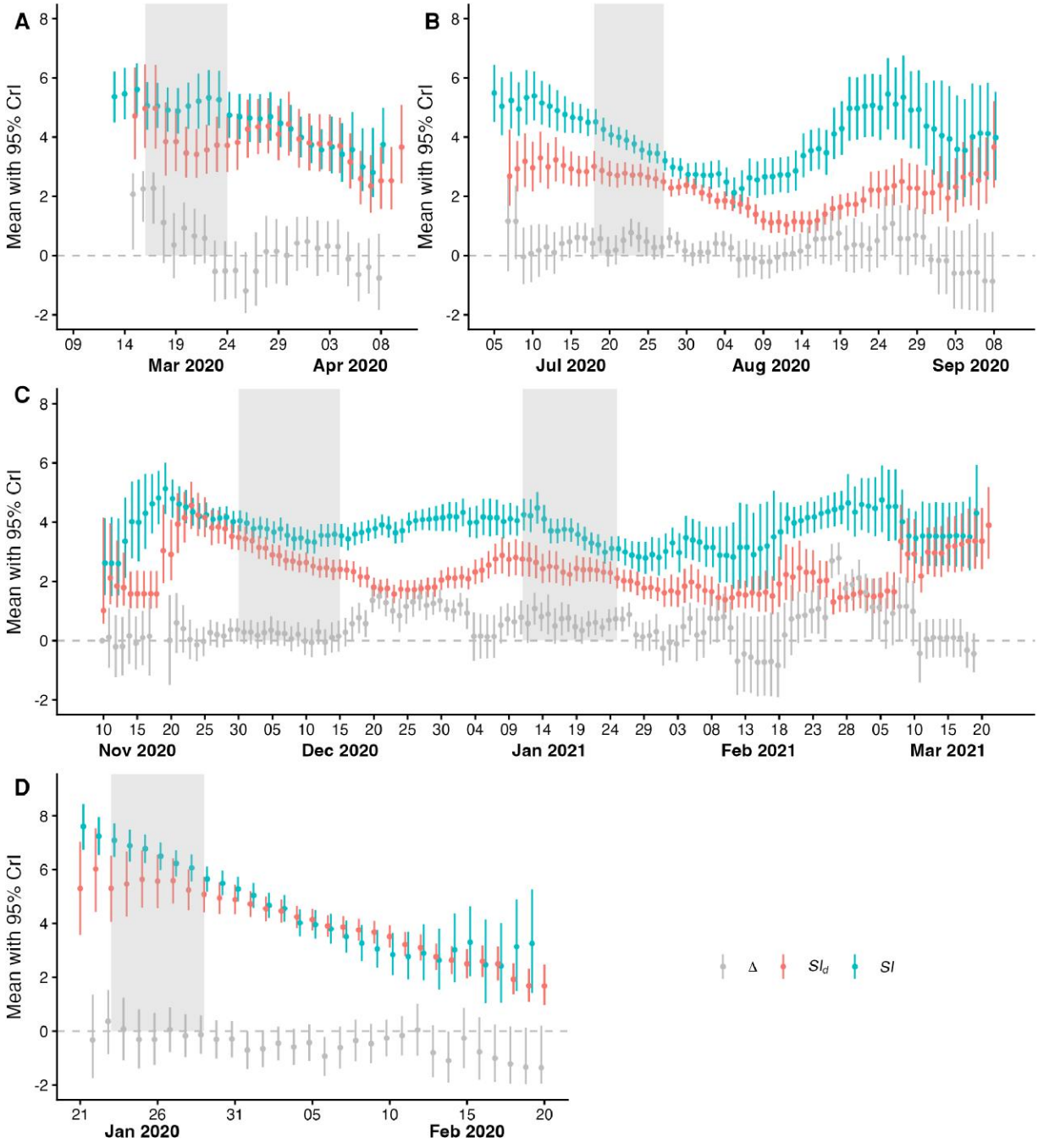


Figure 2. Temporal pattern of diagnostic (SI_d) and clinical (SI) serial intervals and the differences (Δ) between d_1 (time since onset to report for infectors) and d_2 (time since onset to report for infectees) for the second (*A*), third (*B*), and fourth (*C*) pandemic waves in Hong Kong, and first wave in mainland China (*D*). SI was estimated as the interval between successive onsets in the transmission chain (blue points with vertical error lines) and SI_d was the time between diagnostic reporting between cases in transmission pairs (red points with vertical error lines). Δ was estimated as the distributions of observed differences between d_1 and d_2 (gray points with vertical error lines). The points in respective colors represent the estimate of means in each time point considering 10-day sliding windows and the related error bars are the 95% credible intervals (CrI). The shaded rectangles show the epidemic peak periods for the respective waves.

DISCUSSION

Using contact tracing data for COVID-19 across 3 epidemic waves in Hong Kong and the first wave in mainland China, we inferred SI_d and assessed its comparability with SI. Time-varying SI and SI_d produced comparable R_t estimates using both reported and onset-based epicurves (Figure 3). SI_d estimates were generally shorter than SI estimates, consistent with effective contact tracing identifying secondary cases during the initial waves in both locations [33].

Downloaded from academic.oup.com/jid/advance-article/doi/10.1093/infdis/jiag443/8770953 by guest on 06 November 2026

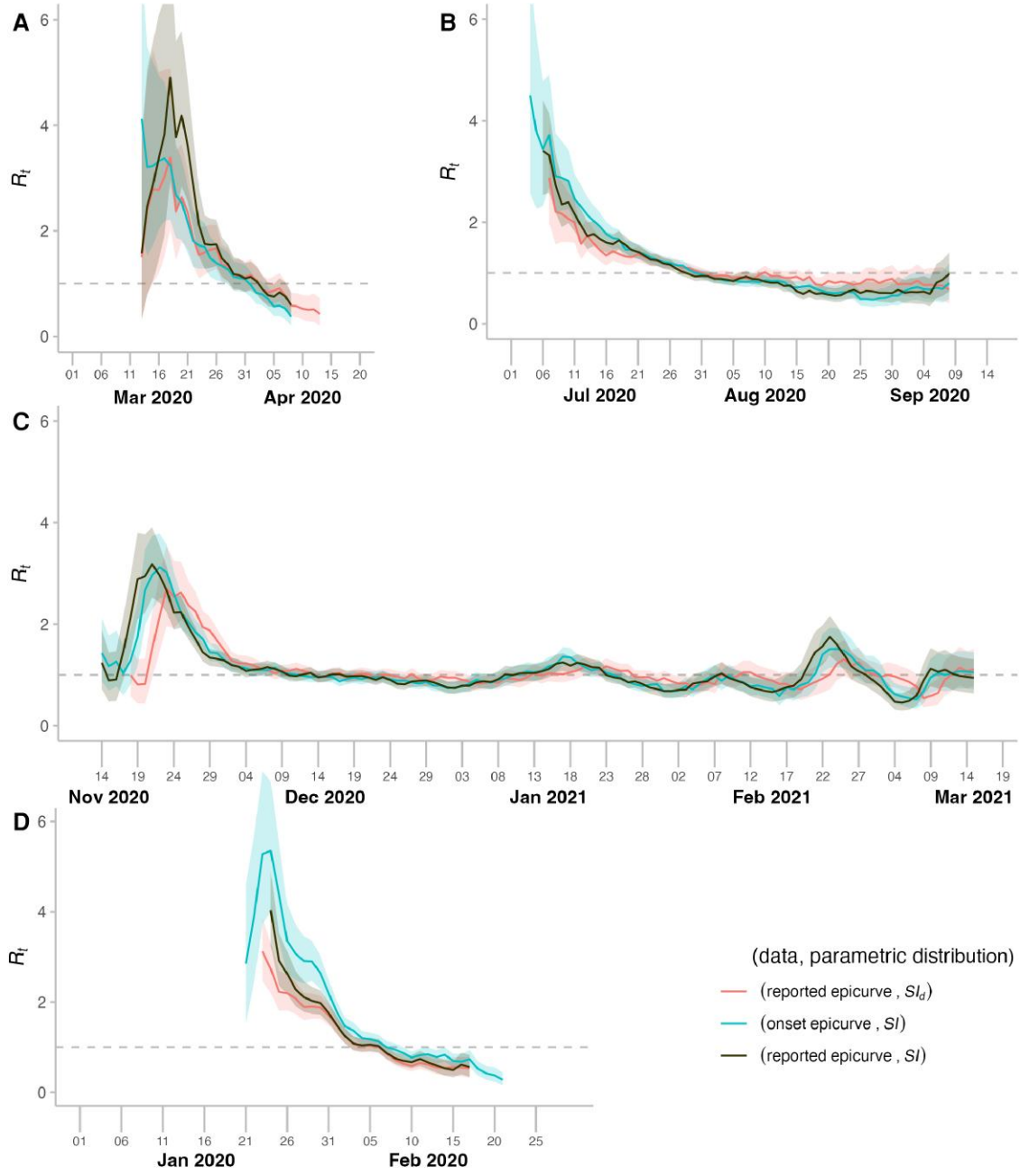


Figure 3. Transmissibility, represented by effective reproduction number R_t, of COVID-19 in Hong Kong in the second (*A*), third (*B*), and fourth (*C*) pandemic waves in Hong Kong, and first wave in mainland China (*D*). The red solid line represents the estimates of R_t based on reported epicurve and the time-varying diagnostic serial interval (SI_d), and the blue solid line was obtained using the onset epicurve and the time-varying clinical serial interval (SI). The black solid line shows the traditional method-based estimates of R_t using reported epicurve and time-varying SI. The respective colored shaded regions are for 95% confidence intervals. The gray dashed line in each panel represents the threshold value of R_t (= 1) when the outbreak was under control in the population.

Even with fixed SI, SI_d varies when reporting delays for infectors and infectees change over time (Supplementary Figure 1). Reporting delay was a key factor driving between-wave variation in SI_d (Supplementary Figure 2). During Hong Kong's third wave and mainland China's first wave, reporting delays followed a unimodal pattern, peaking during epidemic peaks (Supplementary Figure 3), likely reflecting overwhelmed health care and surveillance systems during high case incidence [33]. Beyond reporting delays, SI_d varied with PHSMs, case profiles, and demographics, as reported for SI [12, 16, 28, 29]. In Hong Kong, regression models incorporating reporting delay, isolation delay, severity, household transmission, local case status, and contact tracing explained 69%–92% of SI_d variation (Supplementary Tables 3–5). These findings align with

Downloaded from academic.oup.com/jid/advance-article/doi/10.1093/infdis/jiag443/8770953 by guest on 06 November 2026

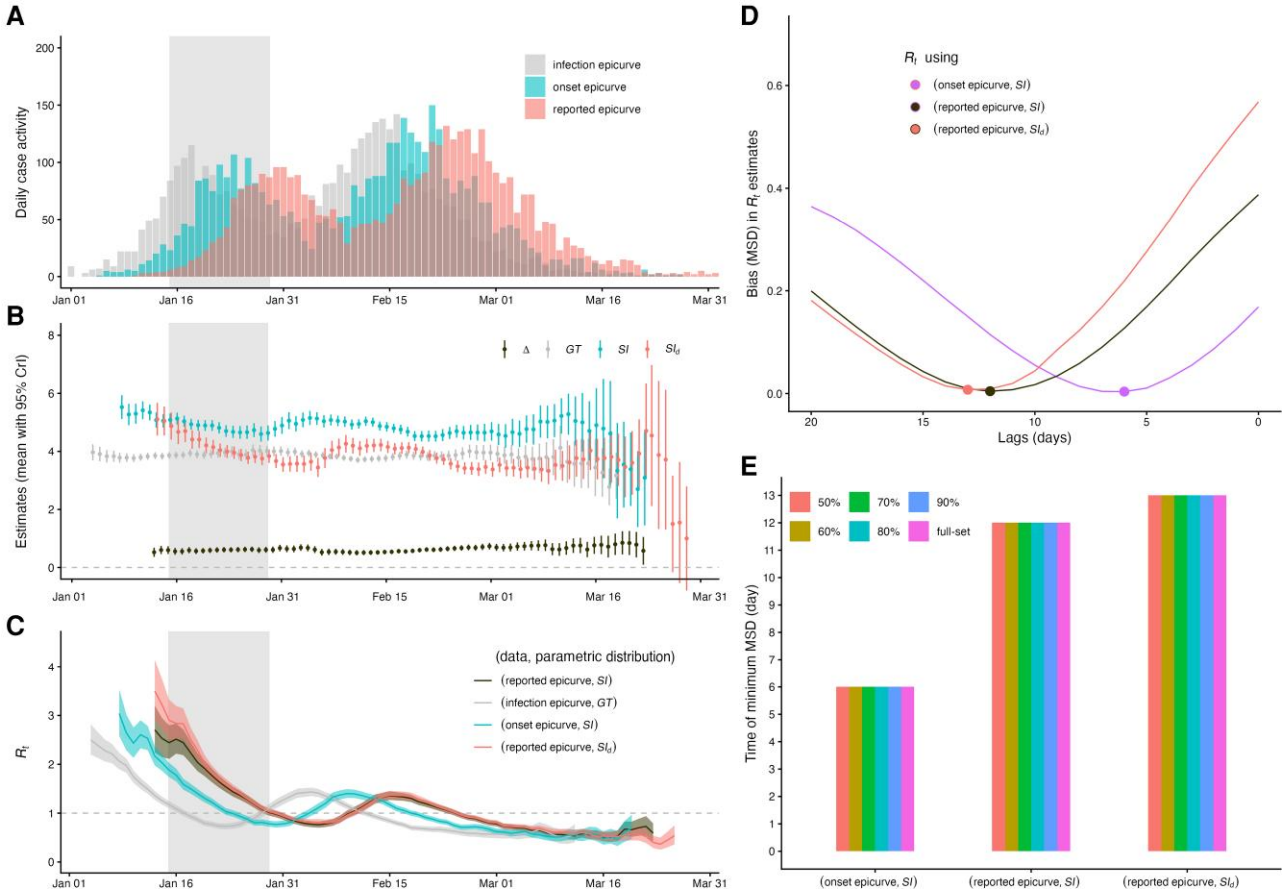


Figure 4. Simulation framework for evaluating the performance of diagnostic serial interval (SI_d) in inferring time-varying transmissibility (R_t) by comparing respective biases with respect to the intrinsic transmissibility under a specific intervention, that is early isolation of the cases after onset. (*A*) Reconstruction of epidemic curves based on the timing of infections, symptom onsets, and reports of cases under 60% intervention effectiveness for early isolation of the cases after onset (additional scenarios in Supplementary Figures 6–8). (*B*) Time-varying estimates of generation time (*GT*, gray points with vertical error lines), serial interval (*SI*, blue points with vertical error lines), and diagnostic serial interval (SI_d, red points with vertical error lines) distributions with mean in respective color points and 95% credible intervals (CrI) shown in the vertical error lines, considering 10-day sliding windows. (*C*) Time-varying reproduction number (R_t) estimated by pairing epidemic curves (based on infection, onset, reporting timings) with parametric distributions of infectiousness (*GT*, *SI*, SI_d). The red solid line represents the estimates of R_t based on reported epicurve and the time-varying SI_d, and the blue solid line was obtained using the onset epicurve and the time-varying *SI*. The black solid line shows the traditional method of estimating R_t based on reported epicurve and time-varying *SI*. The shaded regions are 95% confidence intervals. The gray dashed horizontal line represents the threshold value of R_t when transmissibility was stable in the population. (*D*) Biases in respective R_t estimates quantified as mean squared differences (MSD), calculated relative to the reference intrinsic R_t derived from the infection curve and *GT*. Solid lines indicate the respective biases in R_t estimates for different lags (0–20 days) and dots are the optimal lag time (days) as minimizing MSD. (*E*,) Optimal lag time (days) as minimizing MSD in respective estimated R_t with various length of its timeseries (50% to 100%) to see the sensitivity of the data used. The light-gray shaded regions in panel (A)–(C) are the timing of the intervention period.

evidence that early isolation shortens generation times and serial intervals while increasing presymptomatic transmission [12, 16, 28]. Onset-to-isolation delay emerged as a dominant determinant of outbreak controllability, particularly when R_0 was low (that is below 1) without additional interventions [34]. In early Hong Kong epidemics, approximately 70% of cases were imported or linked to imported cases [35]. Subsequent border controls, quarantine, and enhanced surveillance substantially reduced imported case transmissibility, keeping it below 1 in later waves [36].

When case numbers are low but asymptomatic infection is common (30%–75%) [37–39], small samples may introduce bias, particularly early in outbreaks. In such scenarios, SI_d is particularly useful as it accounts for transmission pairs regardless of symptom status. *SI*-based and SI_d-based estimates yielded similar R_t trajectories, with MAD ranging from 0.05 to 0.23 across waves (Figure 3 and Supplementary Table 6). Disagreements concentrated in the initial phase of each wave when symptom onset ascertainment and reporting delays differed. Reporting delays distort epicurves and bias transmission estimates [40, 41]. For instance, early social distancing relaxation increased R_t from 0.7 to 3.2, whereas reinstatement reduced it only to 1.3 due to confirmation delays burdening contact tracing [42]. Shorter reporting delays during active

Downloaded from academic.oup.com/jid/advance-article/doi/10.1093/infdis/jiag443/8770953 by guest on 06 November 2026

contact tracing associated with shorter SI_d (Figure 4*B*), occurring when intervention effectiveness reached ≥ 60%, substantially affecting R_t estimates.

Recent studies suggest that, for estimating R_t, the forward effective *SI* better approximates *GT* than a constant *SI* [12, 16, 28–30]. Our proposed metric, effective SI_d, can provide comparable R_t estimates when used with the reported epicurve. In theory, for scale of parametric distributions and data, both SI_d paired with the reported epicurve and *SI* paired with the onset epicurve can yield reasonable real-time R_t estimates. However, because *SI* often relies on self-reported symptom onset, effective SI_d may be preferable for real-time estimation using reported case data. Our simulations showed that time-varying R_t estimates based on intrinsic *GT*, effective *SI*, and effective SI_d with their corresponding epicurves followed similar trends across waves, with only temporal bias introduced by the types of data used when case profiles and other factors were held constant in the population during the epidemic (Figure 4 and Supplementary Figure 6). However, variation in case profiles and case-based interventions may still cause magnitude bias in real-time R_t estimates, even when *SI* is used [12, 16, 28, 29].

Accurate estimation of the effective R_t requires the convolution of case data with parametric infectiousness distributions [8, 10, 32], which may vary with epidemic progression [12, 16, 30]. Conventional real-time approaches often rely on simplifying assumptions, such as constant infectiousness or the substitution of *SI* for *GT*, and should therefore be interpreted with caution [32, 43]. Such approximations can introduce bias, potentially underestimating transmissibility and distorting estimates of key epidemiological quantities (eg, *GT*, case fatality rates), particularly during exponential growth phases when right-censoring and multiple potential infectors are not adequately accounted for [12, 44–46]. A further source of bias arises when the reported epicurve is convolved with an *SI* distribution, creating a mismatch in temporal scales. In this study, we aligned the reported epicurve and SI_d to the same reporting timescale, which yields R_t estimates that better reflect real-time transmissibility compared with conventional methods (Supplementary Figures 7 and 8). In general, R_t estimated from the reported epicurve and effective SI_d can be adjusted for temporal biases using time-varying reporting delays and incubation period to better approximate intrinsic transmissibility. When onset data are available, R_t estimation should ideally use the clinical *SI* with onset epicurves for more accurate assessment as both data and parametric distributions are at same time scale (onset timing). However, when only reported case data are available, R_t estimated from reported epicurves and effective SI_d offers a practical alternative, if uncertainties from observation delays and data quality are explicitly modeled and results are interpreted with recognition of inherent reporting delays.

Our study demonstrated that SI_d is a viable alternative to *SI* for estimating time-varying R_t. Although validated using COVID-19 data from Hong Kong and mainland China, generalization to other pathogens requires caution. Several limitations should be acknowledged. First, inferring SI_d requires detailed contact tracing data, which are rarely collected for seasonal respiratory viruses. Second, SI_d is influenced by the efficiency and speed of the detection and reporting system, which can vary depending on the testing strategies employed (eg, rapid antigen tests [RATs] versus polymerase chain reaction [PCR] testing). For instance, during the early stages of the pandemic in Hong Kong, RATs were not widely available [47]; instead, suspected cases were primarily confirmed through PCR testing of nasal or throat samples collected by health care professionals [48]. Consequently, delays in detection and reporting can introduce bias in SI_d estimates. This limitation is particularly pertinent in contexts where health care systems are overwhelmed, or testing capacity is limited. Third, similar to other delay distributions for epidemic parameters (interval measures), SI_d estimates are not free from recall and selection biases, particularly during epidemic growth and shrinkage phases. While selection bias can theoretically be addressed by accounting for the growth rate in the estimation method, this was not the primary goal of our study. Backward-looking serial interval estimates (anchored to the infectee) are subject to right-truncation bias and are highly sensitive to the epidemic growth rate, with intervals measured during exponential growth being systematically shorter and those during declining phases biased upwards [30]. In contrast, the forward-looking approach (anchored to the infector's symptom onset) is less susceptible to these phase-dependent biases and more appropriate for characterizing intrinsic transmission potential [12]. Fourth, similar to *SI*-based R_t estimates, SI_d-based R_t estimates exhibit inherent temporal bias due to reporting delay, in addition to potential recall and selection biases. Our analyses revealed an approximately 1-week lag in detecting changes in transmission dynamics, which was particularly evident when R_t crossed the critical threshold of 1 (Figure 4*C*) with the respective biases (Figure 4*D*). This delay arises because reported cases reflect infections that occurred several days to weeks earlier, compounded by the time required for symptom development, testing, and case reporting. While such temporal bias could be adjusted for under a consistent surveillance system with known reporting delays, inference of reporting delay distributions would be required when such information is unavailable. Fifth, we validated the proposed measure primarily through simulation, comparing reconstructed intrinsic transmissibility with estimates under various data scenarios and assumptions. Although this approach enabled controlled testing, further evaluation using real-world data is needed, particularly for inferring time-varying *GT* from exposure or infection times

Downloaded from academic.oup.com/jid/advance-article/doi/10.1093/infdis/jiag443/8770953 by guest on 06 November 2026

reconstructed from contact tracing and viral load data [12]. Sixth, a normal distribution within the Bayesian framework for estimating time-varying *SI* could account for negative *SI* values, which were significantly smaller in proportion for each temporal windows (7–14 days) in our data across the waves in Hong Kong and mainland China. However, in settings where a substantial proportion of negative serial intervals is present, often due to high uncertainty in transmission pair assignments or longer temporal windows, one should be cautious when considering these negative *SI* values in the inference to avoid significant biases. Finally, further research is needed to investigate the potential impact of factors including vaccination, variant transmissibility, and changes in PHSMs on SI_d.

Despite these limitations, our study highlights the potential utility of SI_d as an alternative to *SI* for estimating the effective R_t and other transmissibility measures for respiratory viruses including COVID-19. However, it is important to emphasize that SI_d is inherently system specific and context dependent. Unlike the clinical serial interval, SI_d is strongly influenced by health care system characteristics and surveillance infrastructure, including testing capacity and accessibility, health care-seeking behavior, contact tracing strategies, and laboratory infrastructure. Therefore, SI_d estimates derived from 1 health care system or time period may not be directly generalizable to other settings. While SI_d does not replace the clinical serial interval as a measure of biological transmission dynamics, it can serve as a pragmatic proxy for monitoring relative trends in transmissibility when onset data are unavailable, provided that results are interpreted with appropriate caution regarding inherent reporting delays. By incorporating both symptomatic and asymptomatic cases, SI_d may offer a more comprehensive understanding of disease transmission characteristics while addressing the limitations and biases associated with self-reported symptom onset data. Further research is essential to validate and refine the application of SI_d across various settings and populations, as well as to explore its potential role in monitoring and controlling the spread of infectious diseases.

Supplementary Data

Supplementary materials are available at *The Journal of Infectious Diseases* online (http://jid.oxfordjournals.org/). Supplementary materials consist of data provided by the author that are published to benefit the reader. The posted materials are not copyedited. The contents of all supplementary data are the sole responsibility of the authors. Questions or messages regarding errors should be addressed to the author.

Notes

Author contributions. S. T. A. and B. J. C. conceived the study and secured funding, with S. T. A. providing overall supervision. Data were curated by M. P. H., A. Y., D. C., W. W. L., F. H., H. G., and S. T. A. Methodology was developed by M. P. H. and S. T. A. Formal analysis and software implementation were conducted by M. P. H. Investigation was carried out by M. P. H., A. Y., D. C., D. C. A., and S. T. A. Visualizations were prepared by M. P. H. and S. T. A. Validation was performed by M. P. H., Y. C. L., and S. T. A. Resources were provided by S. T. A. and B. J. C. The original draft was written by M. P. H. and S. T. A., and the manuscript was reviewed and edited by W. W. L., Y. C. L., J. Y. W., E. H. Y. L., L. W., Z. D., P. W., and B. J. C.

Acknowledgments. The authors thank Julie Au for her technical assistance.

Disclaimer. The funding bodies had no role in study design, data collection and analysis, preparation of the manuscript, or the decision to publish.

Data sharing. All data generated from publicly available sources, codes, and materials will be provided upon specific request to the author.

Financial support. This work was supported by the University of Hong Kong (URC project code 2201100868 to S. T. A.); Health and Medical Research Fund, Hong Kong Administrative Region, China (project number 20190712 to S. T. A.); AIR@InnoHK administered by the Innovation and Technology Commission; and the Research Grants Council, Hong Kong Special Administrative Region, China (project number T11-705/21-N to B. J. C.).

Potential conflicts of interest. B. J. C. consults for AstraZeneca, Fosun Pharma, GSK, Haleon, Moderna, Novavax, Pfizer, Roche, and Sanofi Pasteur. All other authors report no potential conflicts.

All authors have submitted the ICMJE Form for Disclosure of Potential Conflicts of Interest. Conflicts that the editors consider relevant to the content of the manuscript have been disclosed.

References

1. Bi Q, Wu Y, Mei S, et al. Epidemiology and transmission of COVID-19 in 391 cases and 1286 of their close contacts in Shenzhen, China: a retrospective cohort study. Lancet Infect Dis **2020**; 20:911–9.
2. He X, Lau EHY, Wu P, et al. Temporal dynamics in viral shedding and transmissibility of COVID-19. Nat Med **2020**; 26:672–5.
3. Li Q, Guan X, Wu P, et al. Early transmission dynamics in Wuhan, China, of novel coronavirus-infected pneumonia. N Engl J Med **2020**; 382:1199–207.
4. Althobaity Y, Wu J, Tildesley MJ. A comparative analysis of epidemiological characteristics of MERS-CoV and SARS-CoV-2 in Saudi Arabia. Infect Dis Model **2022**; 7: 473–85.
5. Levy JW, Cowling BJ, Simmerman JM, et al. The serial intervals of seasonal and pandemic influenza viruses in

Downloaded from academic.oup.com/jid/advance-article/doi/10.1093/infdis/jiag443/8770953 by guest on 06 November 2026

households in Bangkok, Thailand. Am J Epidemiol **2013**; 177:1443–51.
6. Vink MA, Bootsma MCJ, Wallinga J. Serial intervals of respiratory infectious diseases: a systematic review and analysis. Am J Epidemiol **2014**; 180:865–75.
7. Cauchemez S, Boelle P-Y, Donnelly CA, et al. Real-time estimates in early detection of SARS. Emerg Infect Dis **2012**; 12:110–3.
8. Cauchemez S, Boëlle P-Y, Thomas G, Valleron A-J. Estimating in real time the efficacy of measures to control emerging communicable diseases. Am J Epidemiol **2006**; 164:591–7.
9. Cowling BJ, Ali ST, Ng TWY, et al. Impact assessment of non-pharmaceutical interventions against coronavirus disease 2019 and influenza in Hong Kong: an observational study. Lancet Public Health **2020**; 5:e279–88.
10. Wallinga J, Teunis P. Different epidemic curves for severe acute respiratory syndrome reveal similar impacts of control measures. Am J Epidemiol **2004**; 160:509–16.
11. Wallinga J, Lipsitch M. How generation intervals shape the relationship between growth rates and reproductive numbers. Proc R Soc B: Biol Sci **2007**; 274:599–604.
12. Chen D, Lau Y-C, Xu X-K, et al. Inferring time-varying generation time, serial interval, and incubation period distributions for COVID-19. Nat Commun **2022**; 13:7727.
13. Torneri A, Libin P, Scalia Tomba G, Faes C, Wood JG, Hens N. On realized serial and generation intervals given control measures: the COVID-19 pandemic case. PLoS Comput Biol **2021**; 17:e1008892.
14. Svensson Å. A note on generation times in epidemic models. Math Biosci **2007**; 208:300–11.
15. Leung K, Wu JT, Liu D, Leung GM. First-wave COVID-19 transmissibility and severity in China outside Hubei after control measures, and second-wave scenario planning: a modelling impact assessment. Lancet **2020**; 395:1382–93.
16. Ali ST, Wang L, Lau EHY, et al. Serial interval of SARS-CoV-2 was shortened over time by nonpharmaceutical interventions. Science **2020**; 369:1106–9.
17. Walsh KA, Spillane S, Comber L, et al. The duration of infectiousness of individuals infected with SARS-CoV-2. J Infect **2020**; 81:847–56.
18. Sharker Y, Kenah E. Estimating and interpreting secondary attack risk: binomial considered biased. PLoS Comput Biol **2021**; 17:e1008601.
19. Lydeamore MJ, Campbell PT, Price D J,et al. Estimation of the force of infection and infectious period of skin sores in remote Australian communities using interval-censored data. PLoS Computat Biol **2020**; 16:e1007838.
20. Liu Y, Eggo RM, Kucharski AJ. Secondary attack rate and superspreading events for SARS-CoV-2. Lancet **2020**; 395:e47.
21. Griffin KM, Karas MG, Ivascu NS, Lief L. Hospital preparedness for COVID-19: a practical guide from a critical care perspective. Am J Respir Crit Care Med **2020**; 201:1337–44.
22. Griffin J, Casey M, Collins Á, et al. Rapid review of available evidence on the serial interval and generation time of COVID-19. BMJ Open **2020**; 10:e040263.
23. Gao Z, Xu Y, Sun C, et al. A systematic review of asymptomatic infections with COVID-19. J Microbiol Immunol Infect **2021**; 54:12–6.
24. Mettler SK, Kim J, Maathuis MH. Diagnostic serial interval as a novel indicator for contact tracing effectiveness exemplified with the SARS-CoV-2/COVID-19 outbreak in South Korea. Int J Infect Dis **2020**; 99:346–51.
25. Mefsin YM, Chen D, Bond HS, et al. Epidemiology of infections with SARS-CoV-2 omicron BA.2 variant, Hong Kong, January-March 2022. Emerg Infect Dis **2022**; 28:1856–8.
26. Du Z, Xu X, Wu Y, Wang L, Cowling BJ, Meyers LA. Serial interval of COVID-19 among publicly reported confirmed cases. Emerg Infect Dis J **2020**; 26:1341.
27. Xu X-K, Liu XF, Wu Y, et al. Reconstruction of transmission pairs for novel coronavirus disease 2019 (COVID-19) in mainland China: estimation of superspreading events, serial interval, and hazard of infection. Clin Infect Dis **2020**; 71:3163–7.
28. Ali ST, Chen D, Lau Y-C, et al. Insights into COVID-19 epidemiology and control from temporal changes in serial interval distributions in Hong Kong. Am J Epidemiol **2025**; 194:1079–89.
29. Ali ST, Yeung A, Shan S, et al. Serial intervals and case isolation delays for coronavirus disease 2019: a systematic review and meta-analysis. Clin Infect Dis **2022**; 74:685–94.
30. Park SW, Sun K, Champredon D, et al. Forward-looking serial intervals correctly link epidemic growth to reproduction numbers. Proc Natl Acad Sci U S A **2021**; 118:e2011548118.
31. Lin Y, Wu P, Tsang TK, et al. Viral kinetics of SARS-CoV-2 following onset of COVID-19 in symptomatic patients infected with the ancestral strain and omicron BA.2 in Hong Kong: a retrospective observational study. Lancet Microbe **2023**; 4:e722–31.
32. Cori A, Ferguson NM, Fraser C, Cauchemez S. A new framework and software to estimate time-varying reproduction numbers during epidemics. Am J Epidemiol **2013**; 178:1505–12.
33. Yuan H-Y, Blakemore C. The impact of contact tracing and testing on controlling COVID-19 outbreak without lockdown in Hong Kong: an observational study. Lancet Reg Health—Western Pac **2022**; 20:100374.
34. Kucharski AJ, Klepac P, Conlan AJK, et al. Effectiveness of isolation, testing, contact tracing, and physical distancing on reducing transmission of SARS-CoV-2 in different settings: a mathematical modelling study. Lancet Infect Dis **2020**; 20:1151–60.

Downloaded from academic.oup.com/jid/advance-article/doi/10.1093/infdis/jiag443/8770953 by guest on 06 November 2026

35. Lam HY, Lam TS, Wong CH, et al. The epidemiology of COVID-19 cases and the successful containment strategy in Hong Kong—January to May 2020. Int J Infect Dis **2020**; 98:51–8.
36. Yang B, Lin Y, Xiong W, et al. Comparison of control and transmission of COVID-19 across epidemic waves in Hong Kong: an observational study. Lancet Reg Health—Western Pac **2024**; 43:100969 .
37. Sah P, Fitzpatrick MC, Zimmer CF, et al. Asymptomatic SARS-CoV-2 infection: a systematic review and meta-analysis. Proc Natl Acad Sci U S A **2021**; 118:e2109229118.
38. Nishiura H, Kobayashi T, Miyama T, et al. Estimation of the asymptomatic ratio of novel coronavirus infections (COVID-19). Int J Infect Dis **2020**; 94:154–5.
39. Day M. COVID-19: identifying and isolating asymptomatic people helped eliminate virus in Italian village. BMJ **2020**; 368:m1165.
40. Ma L, Qiu Z, Van Mieghem P, Kitsak M. Reporting delays: a widely neglected impact factor in COVID-19 forecasts. PNAS Nexus **2024**; 3:pgae204.
41. Parag KV, Donnelly CA, Zarebski AE. Quantifying the information in noisy epidemic curves. Nat Comput Sci **2022**; 2:584–94.
42. Yuan H-Y, Blakemore C. The impact of multiple non-pharmaceutical interventions on controlling COVID-19 outbreak without lockdown in Hong Kong: a modelling study. Lancet Reg Health—Western Pac **2022**; 20:100343.
43. Gostic KM, McGough L, Baskerville EB, et al. Practical considerations for measuring the effective reproductive number, Rt. PLoS Computat Biol **2020**; 16: e1008409.
44. Britton T, Scalia Tomba G. Estimation in emerging epidemics: biases and remedies. J R Soc Interface **2019**; 16: 20180670.
45. Charniga K, Park SW, Akhmetzhanov AR, et al. Best practices for estimating and reporting epidemiological delay distributions of infectious diseases. PLoS Computat Biol **2024**; 20:e1012520.
46. Park SW, Sun K, Abbott S, et al. Inferring the differences in incubation-period and generation-interval distributions of the Delta and Omicron variants of SARS-CoV-2. Proc Natl Acad Sci U S A **2023**; 120:e2221887120.
47. Du Z, Tian L, Jin D-Y. Understanding the impact of rapid antigen tests on SARS-CoV-2 transmission in the fifth wave of COVID-19 in Hong Kong in early 2022. Emerg Microbes Infect **2022**; 11:1394–401.
48. Zhan W. Hong Kong to switch to throat swabs for PCR tests starting Nov 8, 2022. Asia News Network. https://asianews.network/hong-kong-to-switch-to-throat-swabs-for-pcr-tests-starting-nov-8/. Accessed 12 May 2023.

Downloaded from academic.oup.com/jid/advance-article/doi/10.1093/infdis/jiag443/8770953 by guest on 06 November 2026